Theor Chem Acc (2012) 131:1296
DOI 10.1007/s00214-012-1296-6

REGULAR ARTICLE

# A computational study toward understanding the separation of ions of potassium chloride microcrystal in water

**Anik Sen · Bishwajit Ganguly**

Received: 23 March 2012 / Accepted: 24 October 2012


**Abstract** The dissolution phenomenon of potassium chloride microcrystal in water has been studied using DFT calculations and molecular dynamics studies. DFT study reveals the departure of $Cl^-$ to be more pronounced from the edge positions compared to the corner sites of the KCl $[(KCl)_6(H_2O)_n$, $n = 1$–$15]$ microcrystal lattice. The dissolution initiates through the movement of a $Cl^-$ from the edge of the crystal lattice (5.19 Å) at $n = 4$ water molecules in agreement with the separation of ions from a single KCl molecule. This separation is more evident with the cluster of 6 water molecules (6.12 Å). The characteristics of KCl dissolution dynamics, such as the sequential departure of ions from the crystal, the hydrated ions and the dynamical role of the water molecules, are further studied by classical molecular dynamics simulations employing GROMACS force field. Molecular dynamics calculations are performed with a larger crystal of KCl with {100} plane consisting of 108 $K^+$ and 108 $Cl^-$ ions. The MD studies have been extended with relatively unstable planes of KCl {110} (consisting of 105 $K^+$ and 105 $Cl^-$ ions) and {111} (consisting of 120 $K^+$ and 120 $Cl^-$ ions). The simulations revealed that the dissolution of {110} and {111} planes is relatively faster than that of the stable {100} plane. A mean square displacement analysis also supported this observation. The dissolution of the ions generally occurs from the top layer of {100} surface, while other layers remain intact. However, such a definite pattern of dissolution is not noticed with {110} and {111} planes.

**Keywords** Solvation · KCl microcrystal · DFT · Molecular dynamics · Mean square displacement

## 1 Introduction

The study of solvation phenomena in inorganic salts is of fundamental importance for theoretical, experimental and economic reasons. These studies have been performed for decades; however, the organization of the molecules in such solution is still not well understood. In this regard, the dissociation of alkali halide salts has become a major interest in solvation chemistry [1–18]. The dissolution of sodium chloride, one of the most important alkali halides, has been studied at both molecular and crystal levels [19–26]. Monte Carlo simulations were performed by Asada et al. [24] on LiCl and NaCl in water to explore the mechanism for the dissociation phenomenon of such salts. Ohtaki et al. [25] studied the dissolution of an NaCl crystal with {111} and {−1−1−1} faces using molecular dynamics simulation and concluded that repulsive forces arising between the chloride ions and the water molecules push the chloride ion out from the crystal surface as they possess smaller hydration energy than the sodium ions. When an ionic crystal is dissolved in water, the surface of the crystal gets covered with water molecules, and the cations and anions leave the surface of the crystal and disperse into the aqueous phase. The dissolution process involves a 'tug of war' between the ionic bonds and the hydration of these ions. The solvation process of sodium chloride at the molecular level showed that a cluster of six

**Electronic supplementary material** The online version of this article (doi:10.1007/s00214-012-1296-6) contains supplementary material, which is available to authorized users.

A. Sen · B. Ganguly (✉)
Analytical Discipline and Centralized Instrument Facility, Central Salt and Marine Chemicals Research Institute (Council of Scientific Industrial Research), Bhavnagar, Gujarat 364 002, India
e-mail: ganguly@csmcri.org

Published online: 09 November 2012

water molecules is necessary to achieve the solvent-separated ion pair of NaCl [19]. Furthermore, the dissolution of sodium chloride crystal in water studied by molecular dynamics simulations indicated that a chloride ion at the corner of the crystal dissolves first [22]. Liu et al. [23] gave a detailed description about the process involved behind the dissolution of the $Na^+$ and $Cl^-$ ions from the NaCl crystal surface. To the best of our knowledge, theoretical studies on the dissolution phenomenon of potassium chloride crystals are still scarce [27].

Recently, we have reported the dissolution process of a single potassium chloride molecule [28], finding that orientations of the water molecules around the potassium chloride seem to be important in the dissociation phenomena. The separation of $K^+$ and $Cl^-$ ions with 4 water molecules adopts a prismatic structure with the K–Cl distance of 4.4 Å, while the largest separation of $K^+$ and $Cl^-$ ions (4.97 Å) was achieved with 6 water molecules in a cubic structure [28]. Though the progress of dissociation of single KCl molecule has been studied, the investigation toward the dissolution of KCl crystal is warranted. In this article, we have explored the dissolution of KCl microcrystal which will also be relevant toward the study of salts in water clusters in environmental chemistry, atmospheric chemistry and cloud physics [29–33].

From saturation concentration, it can be deduced that on average, 15 water molecules are necessary to dissociate a single KCl molecule at 273 K (Supporting Information, Scheme S1), whereas previous theoretical studies by our group suggested that the dissolution of a single KCl molecule starts with only 4 water molecules [28]. In this article, we have explored the number of water molecules needed to start the dissolution and also the progressive solvation of the ions in a microcrystal lattice. Scheme 1 shows the separation of KCl into $K^+$ and $Cl^-$ ions from the crystal lattice in the presence of water molecules. The dissolution process can start either from the corner or from the edge of the microcrystal surface.

We have examined the solvation process of the microcrystal $(KCl)_6$ {100} cluster using DFT calculations consisting of 0–15 water molecules. The progressive dissociation of KCl microcrystal with increasing number of water molecules at the corner and the edge sites of the crystal lattice has been investigated in a systematic way.

The DFT results suggest that 4 is the minimum number of water molecules required to initiate the departure of the $Cl^-$ ions from the KCl microcrystal ($K^{+\cdots}Cl^- = 5.19$ Å), and similar to the dissolution of a single potassium chloride molecule, six water molecules augment the situation (6.12 Å) [28]. The separation of $K^{+\cdots}Cl^-$ increases to ~8.0 Å with 14 water molecules. The simultaneous removal of more than one chloride ion from different sites seems to be less effective in comparison with the removal of a single $Cl^-$ ion from the KCl lattice. The dissociation of ions from the crystal lattice with the solvent molecules occurs with a number of steps: first is the formation of a solvent-shared ion pair, where only one solvent molecule separates the two ions. Dissociation then occurs via solvent-separated ion pairs, where the ion pairs are separated with more than one solvent molecule. However, a clear experimental distinction between these two stages is not easily made [34]. The circumstances under which these thermodynamically distinct species can exist in the solution have been reviewed by Marcus [1].

The finite cluster environment toward the salt dissociation process may vary from the dissolution in the bulk environment [35]. To examine the bulk dissolution process of KCl, classical molecular dynamics simulation studies are performed with the GROMACS 3.3.2 using the GROMOS96 43a1 force field with TIP4P water solvation model. The KCl crystal consists of three most important planes, {100}; {110} and {111} (Scheme 2). Molecular dynamics calculations were performed to examine the dissolution of {100} surface of KCl, and also extended with the less stable surfaces {110} and {111}. The arrangements of the potassium and chloride ions in the three different surfaces are shown in Scheme 2.

In the initial stage of the MD simulation, the elongation of a corner $Cl^-$ ion and a corner $K^+$ ion from the surface lattice is observed, and subsequently, the separation of an ion pair is noticed. The formation of ion pairs shows an agreement with the study of dissolution of sodium chloride in water using flicker-noise spectroscopy (FNS) [36]. Additionally, at longer time scales, the ions separate from the crystal lattice either in the form of ion pair or individual-solvated ions. The top layer of the KCl crystal lattice seems to dissolute, while the other layers remain intact in the crystal lattice. The {110} KCl plane shows separation of an edge ion pair, and the {111} plane showed corner and edge $Cl^-$ ions dissolution in the initial stage of the simulation process. The dissolution of these surfaces is much faster compared to the stable {100} surface. The ions separate from the different sites of the crystal lattice much more easily. It is known from the surface energy calculations that {100} plane of alkali halides is more stable compared to other planes such as {110} and {111} [37–41]. The MSD calculations also support the stability of the {100} plane compared to other planes.

## 2 Computational methods

### 2.1 DFT calculations

DFT calculations were performed with {100} $(KCl)_6(H_2O)_n$ [$n = 0$–15] cluster using the generalized gradient

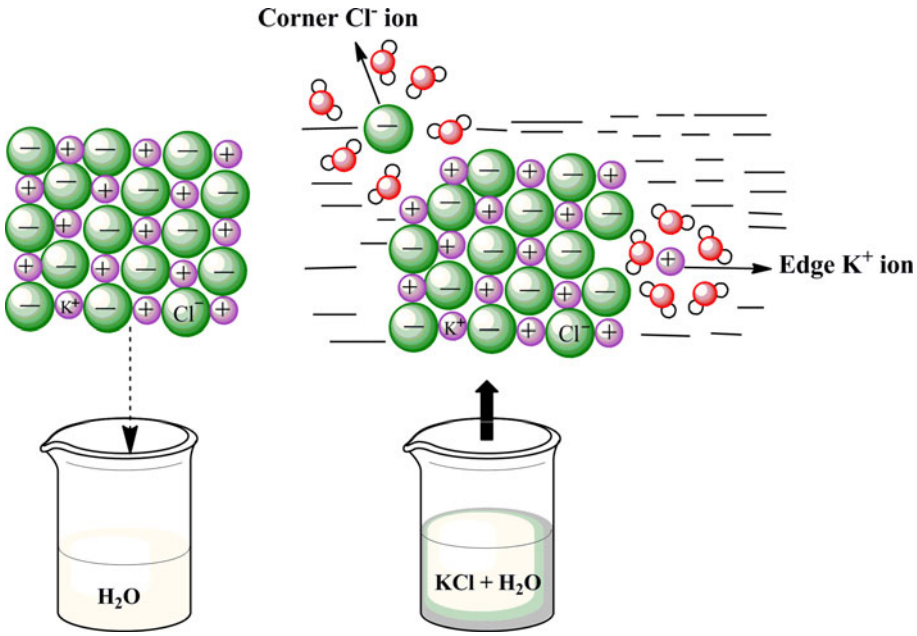


**Scheme 1** The separation of ions from the corner or the edge positions of the lattice. Potassium—*purple*; chlorine—*green*; oxygen—*red*; hydrogen—*white*

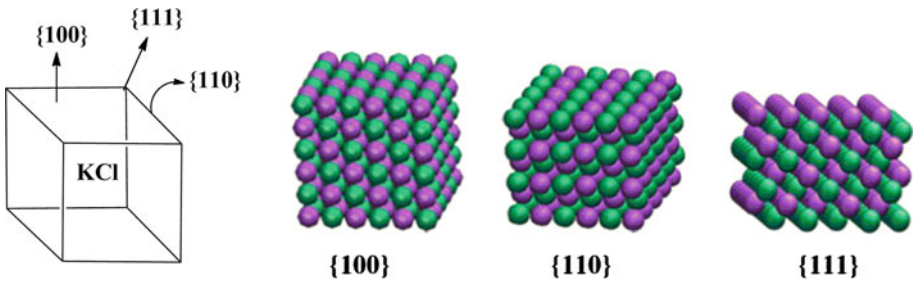


**Scheme 2** The arrangement of potassium and chloride ions on the {100}, {110} and {111} planes of the KCl crystal (*green*: chloride; *purple*: potassium)

approximations (GGAs), which includes density gradients [42–49] along with the functional PW91 [43] employing the density functional program DMol$^3$ in Materials Studio version 4.1.2 of Accelrys Inc., the electronic wave functions were expanded in atom-centered basis functions defined on a dense numerical grid [50–53]. We used the double numerical basis set DND which is comparable with 6-31G* basis set. Single point calculations at Becke's three-parameter exchange functional with the correlation functional of Lee, Yang and Parr with 6-311 + G (2d,p) [22, 54–56] level of theory are performed on the GGA/PW91/DND-optimized geometries using the following equation (Eq. 1) as performed by Yamabe et al. [22] with Gaussian 09, Revision B.01 [57]. The KCl {100} microcrystal for the DFT calculations was prepared using X-ray crystal structure data (Fig. 1) [58].

$$\text{B.E.}(\Delta E) = \left[E\left\{(\text{KCl}_6)(\text{H}_2\text{O})_n\right\} - \left\{E(\text{water}) + E\,\text{of the most stable}\left\{(\text{KCl}_6)(\text{H}_2\text{O})_{n-1}\right\}\right] \quad (1)$$

To examine the effect of entropic contributions to the dissolution process of KCl with water clusters, additional

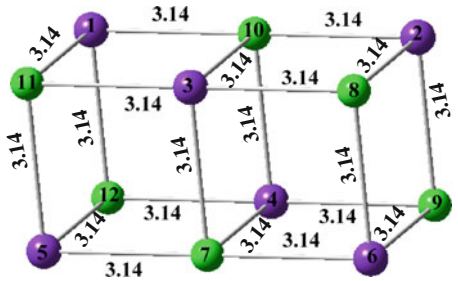


**Fig. 1** The KCl microcrystal taken for the DFT calculations. All distances are given in Å (potassium—*purple*; chlorine—*green*)

free energy calculations were performed using B3LYP/6-311 + G(2d,p)//GGA/PW91/DND level of theory for $[(\text{KCl})_6(\text{H}_2\text{O})_{n\ =1-6}]$. The relative free energy values ($\Delta G$) for the respective clusters are shown in each figure.

## 2.2 Molecular Dynamics Calculations

Molecular dynamics calculations are performed with GROMACS 3.3.2 [59] using GROMOS96 43a1 force field [60]. The simulation supercell of the {100} plane consists of 108 $K^+$ and 108 $Cl^-$ ions in a cubic box surrounded by

3248 water molecules. The {110} and {111} KCl crystals consist of 210 (105 $K^+$ ions and 105 $Cl^-$ ions) and 240 (120 $K^+$ ions and 120 $Cl^-$ ions) atoms, respectively. Similarly, water molecules are placed around the {110} and {111} crystal planes (3,249 water molecules surrounding {110} and 3,238 water molecules surrounding {111} planes). The water–water interaction is described by the TIP4P solvation model [61–63] provided by GROMACS 3.3.2 [59]. The initial cubic simulation boxes for the {100}, {110} and {111} planes of the KCl microcrystal lattice were generated with linear dimensions of 47.236, 47.216 and 47.447 Å, respectively. In all cases, an initial minimization of 100 ps was followed by an equilibration at 300 K for a period of 200 ps. Harmonic restraints on the KCl crystal coordinates are used during the equilibration procedure. The KCl {111} plane is electrostatically highly polar [64–66], and hence the ions get scattered during initial minimization step. Therefore, the ions were kept fixed in all directions during the initial minimization; however, the constraints were removed during the equilibration process. The simulation was performed with the NPT ensemble. The isothermal isobaric simulation (i.e. NPT ensemble dynamics) protocol comprises three major steps: (1) energy minimization of the KCl crystal in bulk water, (2) equilibration run at a desired temperature with harmonic restraints on the KCl crystals and (3) the full molecular dynamics run or production run. The temperature was set to 300 K and at a pressure of 1 atm. Temperature and pressure are kept constant with the coupling constants of 0.1 and 0.5 ps, respectively, by the Berendsen scheme [67]. A periodic boundary condition is applied. The time step used in the simulations was 0.5 fs, and the total time for the molecular dynamics run was 2.5 ns. For electrostatic interactions, we used the particle mesh Ewald method [68, 69]. For potassium and chloride ions, the parameters are taken from the originally developed and supplied within the GROMACS software [60, 70, 71]. Mean square displacement was calculated from the GROMACS 3.3.2 software, as described in earlier studies [72–74]. The KCl crystal structure with the {100}, {110} and {111} surfaces for the MD simulations was also prepared using the X-ray crystal structure data (Fig. 11) [58].

## 3 Results and discussions

The calculated geometrical parameters of $K^{+\cdots}H_2O$ and $Cl^{-\cdots}H_2O$ with GGA/PW91/DND and B3LYP/6-311 + G(2d,p) levels of theory are given in Table 1. The $O^{\cdots}H$ distance and the ∠HOH angle are also given in Table 1 so that the computational methods can be compared with the available experimental data. The energies calculated using B3LYP/6-311 + G(2d,p) are found to be in better agreement with the available experimental results (Table 1). To minimize the computational cost, the single point calculations are performed with B3LYP/6-311 + G(2d,p) on GGA/PW91/DND-optimized geometries, which also provided the similar energetics to those obtained with B3LYP/6-311 + G(2d,p)-optimized results (Table 1). Additionally, the interactions between $K^+$ ion and $Cl^-$ ion with water molecules were also calculated with the GROMOS96 43a1 force field with GROMACS 3.3.2 software [57, 58]. The interactive distances between the water molecule and $K^+$; $Cl^-$ ions are found to be similar with the B3LYP-optimized geometries (Table 1). The interaction of separated ions with the water molecule provides a direct comparison of the experimental data with the computational methods used in this study, which, however, is not available for $KCl^{\cdots}H_2O$ cluster.

### 3.1 DFT calculations

#### *3.1.1 Solvation of KCl microcrystal with 1-6 water molecules*

To examine the solvation phenomenon of KCl crystals, we have considered a microcrystal $(KCl)_6$ surrounded with water molecules. At first, approach of a single water molecule to the $(KCl)_6$ microcrystal is considered. Three different isomeric structures are observed (Fig. 2). The relative interaction energies calculated with B3LYP/6-311 + G(2d,p)//GGA/PW91/DND using Eq. 1 suggest that 2a is more stable than 2b and 2c by 4.0 kcal/mol and 2.8 kcal/mol, respectively (Fig. 2). Furthermore, the free energies calculated for these clusters 2a–2c also showed the similar energetic preferences as observed with the electronic energies. In 2a, the water molecule interacts with $K^+$ and $Cl^-$ ions at the corner of the $(KCl)_6$ microcrystal. The calculated structure 2b showed the interaction of the water molecule with a single $K^+$ ion at the corner of the microcrystal, whereas, in 2c, the water molecule sits in the edge of the surface, weakly interacting with a $K^+$ ion and forming a strong hydrogen bond with the neighboring $Cl^-$ ion (Fig. 2). The approach of single water molecule toward the surface of KCl does not affect the K–Cl distance significantly. The largest separation of $K^+$ and $Cl^+$ ions (3.35 Å) is observed with 2c.

Four different geometries of KCl microcrystal interacting with two water molecules were predicted. In Fig. 3, two structures of $(KCl)_6(H_2O)_2$ are shown and the other two isomers are given in Supporting Information (Figure S1). In the geometry 3b, one of the water molecules binds at the corner potassium ion and other interacts with the edge potassium ion in the KCl microcrystal (Fig. 3). These two water molecules form hydrogen bonds with the same chloride ion (3b, Fig. 3). The K–Cl distance is elongated to

**Table 1** Calculated and experimental structural parameters along with energies for the interaction of KCl with water are given

| Properties | Optimized at GGA/PW91/DND | Single point calculations at B3LYP/6-311 + G(2d,p) with GGA/PW91/DND geometries | Optimized at B3LYP/6-311 + G(2d,p) | Minimized with GROMOS force field | Experimental values |
|---|---|---|---|---|---|
| $r_{OH}$ | 0.977 Å | 0.977 Å | 0.963 Å | 1.00 Å | 0.957 Å [75] |
| ∠HOH | 103.409° | 103.409° | 105.228° | 105.00° | 104.5 [31, 76, 77] |
| $r_{K+...OH2}$ | 2.699 Å | 2.699 Å | 2.62 Å | 2.61 Å | – |
| $r_{Cl...HOH}^{-}$ | 2.052 Å | 2.052 Å | 2.16 Å | 2.13 Å | – |
| B.E. ($K^{+}\cdots OH_2$) | 21.66 kcal/mol | 18.24 kcal/mol | 18.08 kcal/mol | | 17.9 kcal/mol [78] |
| B.E. ($Cl^{-}\cdots HOH$) | 24.71 kcal/mol | 12.83 kcal/mol | 14.7 kcal/mol | | 14.9 kcal/mol [30] |

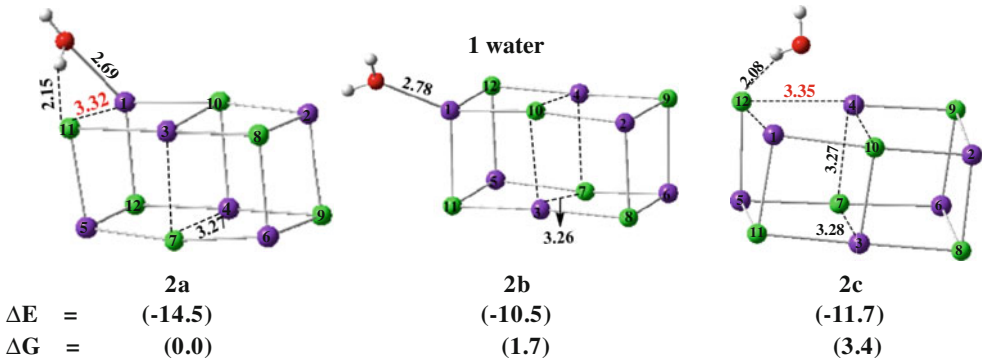


**Fig. 2** B3LYP/6-311 + G(2d,p)//GGA/PW91/DND calculated geometries and binding energies (ΔE) of $(KCl)_6(H_2O)_1$ are given in kcal/mol. The relative free energies (ΔG) at 298 K are given in kcal/mol. All distances are given in Å (potassium—*purple*; chlorine—*green*; oxygen—*red*; hydrogen—*white*)

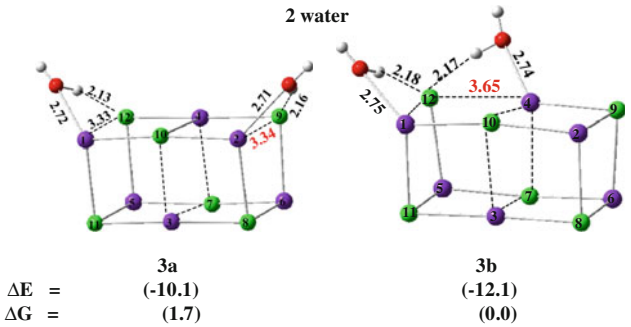


**Fig. 3** B3LYP/6-311 + G(2d,p)//GGA/PW91/DND calculated geometries and binding energies (ΔE) of $(KCl)_6(H_2O)_2$ are given in kcal/mol. The relative free energies (ΔG) at 298 K are given in kcal/mol. Binding energies are calculated with Eq. 1. All distances are given in Å (potassium—*purple*; chlorine—*green*; oxygen—*red*; hydrogen—*white*)

3.65 Å from the edge potassium ion in the KCl cluster. The isomer 3a showed a marginal separation of K–Cl distance compared to the unhydrated KCl crystal (Figs. 1, 3).

Five different solvated structures of $(KCl)_6(H_2O)_3$ have been observed. In geometry 4a, all the three water molecules interact with a single potassium ion (Fig. 4). This structure suggests the elongation of three pairs of K–Cl distance (∼3.44 Å) from the KCl crystal distance of 3.13 Å. Isomer 4b is remarkable in terms of the separation of the $K^{+}\cdots Cl^{-}$, where the water molecules approach from the different sites of the $(KCl)_6$ crystal (Fig. 4). The K–Cl distance in the crystal lattice $K_4$-$Cl_{10}$, $K_3$–$Cl_{10}$ and $K_4$–$Cl_7$ is elongated by more than 4.5 Å. Therefore, the increase in the K–Cl distance is ∼1.37Å compared to the unhydrated KCl microcrystal. These ion pairs separated with water molecules can be considered as solvent-shared ion pair [1, 34]. The similar approach of three water molecules at the corner of KCl microcrystal does not show any significant separation of ions (3.42 Å) (4c, Fig. 4). The other two less stable isomers are given in the Supporting Information (Figure S2).

Three isomeric structures of $(KCl)_6(H_2O)_4$ are shown in Fig. 5. In the calculated geometry 5a, 4 water molecules approach the same face of KCl microcrystal and the water molecules are hydrogen bonded to each other (Fig. 5). This arrangement of water molecules seems to provide the overall stability of the structure, but the separation of $K^{+}$ and $Cl^{-}$ ions is marginal compared to the unhydrated KCl microcrystal. In the case of 5b, 4 water molecules approached from 3 different sites of the KCl microcrystal

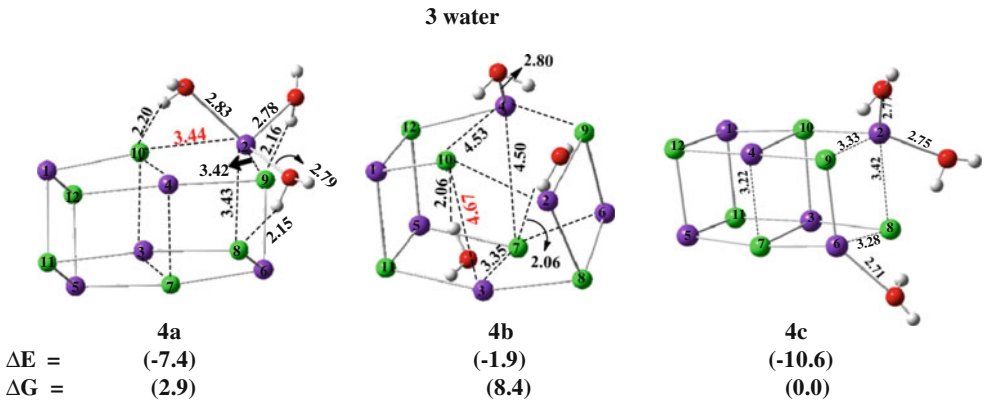


**Fig. 4** B3LYP/6-311 + G(2d,p)//GGA/PW91/DND calculated geometries and binding energies (ΔE) of $(KCl)_6(H_2O)_3$ are given in kcal/mol. The relative free energies (ΔG) at 298 K are given in kcal/mol. Binding energies are calculated with Eq. 1. All distances are given in Å (potassium—*purple*; chlorine—*green*; oxygen—*red*; hydrogen—*white*)

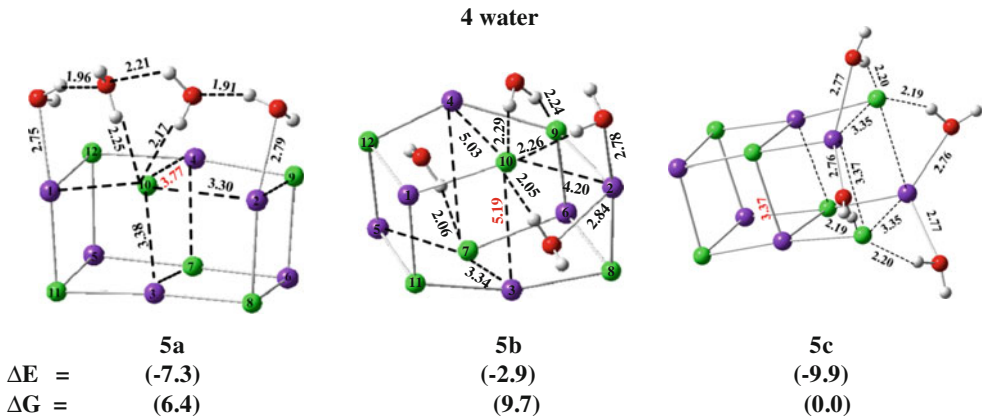


**Fig. 5** B3LYP/6-311 + G(2d,p)//GGA/PW91/DND calculated geometries and binding energies (ΔE) of $(KCl)_6(H_2O)_4$ are given in kcal/mol. The relative free energies (ΔG) at 298 K are given in kcal/mol. Binding energies are calculated with Eq. 1. All distances are given in Å (potassium—*purple*; chlorine—*green*; oxygen—*red*; hydrogen—*white*)

lattice and interacted with the two edge chloride ions, showing a significant movement of the $Cl^-$ ions (Fig. 5). The $K_4$–$Cl_{10}$ and $K_3$–$Cl_{10}$ distances increase to ~5.0 Å, whereas $K_2$–$Cl_{10}$ and $K_4$–$Cl_7$ distances elongate to over 4.0 Å (Fig. 5). The geometry 5c shows the orientation of the water molecules around the $Cl^-$ ion at the corner and it is the most stable structure with 4 water molecules; however, no significant changes are observed in the K–Cl distance (Fig. 5). The relative free energy calculations also showed that 5c is more stable than 5a and 5b. The other calculated geometries are given in the Supporting Information (Figure S3)

The isomeric structure 6a is more stable than the other KCl microcrystal with 5 water molecules 6b and 6c, respectively (Fig. 6). In 6a, four of the water molecules are hydrogen bonded with each other and the fifth one interacts with another $K^+$ and $Cl^-$ ion from a different site. A clear departure of a corner $Cl^-$ ion from the two neighboring potassium ions ($K_4$ and $K_2$) is observed in the case of 6b with distance of 5.0 Å and 4.1 Å, respectively. The hydrated structure 6c shows a similar separation of $Cl^-$ ion from the edge position of KCl microcrystal as observed in the case of 5b. In this case, all the 5 water molecules are hydrogen bonded with the edge chloride ion on the same surface of the KCl microcrystal lattice. This chloride ion ($Cl_7$) is moved away from the crystal lattice, and the distances from the four neighboring potassium ions $K_3$, $K_4$, $K_5$ and $K_6$ being 5.87, 4.45, 4.38 and 4.35 Å, respectively; thus, these can be considered as solvent-shared ion pairs [1, 34]. The other geometries are given in the Supporting Information (Figure S4).

The separation of $K^+$ and $Cl^-$ is found to be 6.12 Å with 6 water molecules (7a, Fig. 7). The chloride ion ($Cl_{10}$) is hydrogen bonded with five water molecules, and the sixth water molecule assists through bridging for better interaction. It appears that the sixth water molecule catalyzes the separation of ions in this case. The other separated distances of the $Cl^-$ ion from the potassium ions $K_1$, $K_2$ and $K_3$ are 4.90, 4.16 and 4.50 Å, respectively. The more stable structure 7b does not show any significant elongation of the KCl distances (7b, Fig. 7). The other geometries of the $(KCl)_6(H_2O)_6$ given in the Supporting Information showed much smaller distances between the $K^+$ and $Cl^-$ ions (Figure S5).

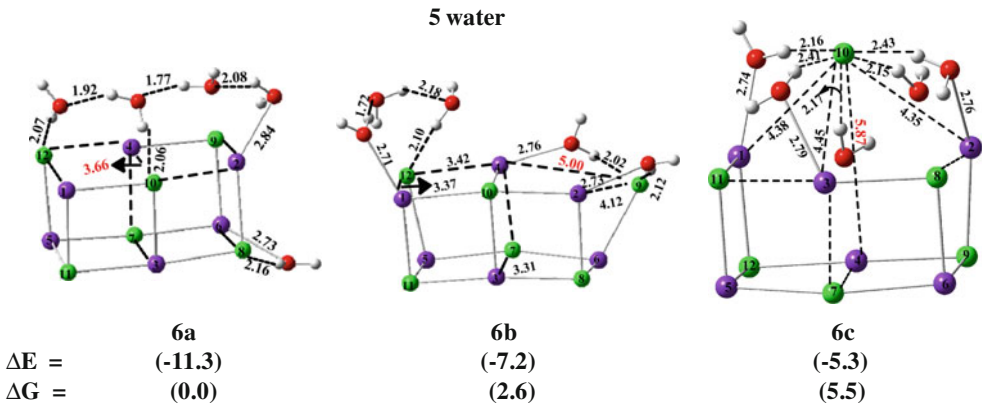


**Fig. 6** B3LYP/6-311 + G(2d,p)//GGA/PW91/DND calculated geometries and binding energies (ΔE) of $(KCl)_6(H_2O)_5$ are given in kcal/mol. The relative free energies (ΔG) at 298 K are given in kcal/mol. Binding energies are calculated with Eq. 1. All distances are given in Å (potassium—*purple*; chlorine—*green*; oxygen—*red*; hydrogen—*white*)

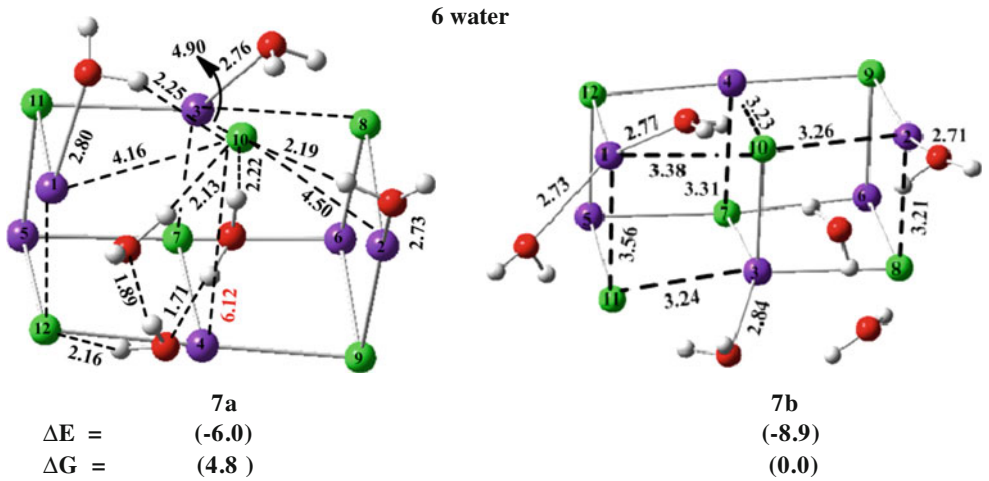


**Fig. 7** B3LYP/6-311 + G(2d,p)//GGA/PW91/DND calculated geometries and binding energies (ΔE) of $(KCl)_6(H_2O)_6$ are given in kcal/mol. The relative free energies (ΔG) at 298 K are given in kcal/mol. Binding energies are calculated with Eq. 1. All distances are given in Å (potassium—*purple*; chlorine—*green*; oxygen—*red*; hydrogen—*white*)

### *3.1.2 Solvation of KCl microcrystal with 7-15 water molecules*

To examine the influence of more number of water molecules on the separation of ions in KCl microcrystal, interactions up to 15 water molecules have been evaluated. Solvent-shared ion pairs are observed with 7, 8 and 9 water clusters upon interaction with the KCl microcrystal lattice. The edge $Cl^-$ showed the separation maximum to 7.10 Å from the lattice with 9 water molecules (8c, Fig. 8).

The addition of a tenth water molecule leads to the further separation of $K^+$ and $Cl^-$ ions (7.50 Å) in the microcrystal lattice of KCl (9a, Fig. 9). It has been observed that at a cluster of at least 4 water molecules around the $K^+$ and $Cl^-$ ions (5b) initiates the separation of the $K^{+\cdots}Cl^-$ (Fig. 5) and 6 water molecules augment the situation (7a, Fig. 7). Therefore, there is another possibility that two water clusters of 4 and 6 water molecules can approach at two different sites of the microcrystal lattice (Scheme 3). The clusters of 4 and 6 water molecules are placed near the edge $Cl^-$ ions at the diagonal positions in the crystal lattice in one case (a, Scheme 3) and in another situation in the edge and a corner $Cl^-$ ion (b, Scheme 3). The two situations show the separation of the ions from the KCl crystal lattice up to 6.29 Å in 9b and 6.79 Å in 9c, respectively; however, such separation of ions is smaller than that of 9a (Fig. 9). Separation of the corner $Cl^-$ ions is not observed. The B3LYP/6-311 + G(2d,p) calculated energies using Eq. 1 suggests that the separation of ions is more preferred in 9a compared to 9b and 9c.

Furthermore, departure of the $Cl^-$ ions from the edge of the lattice is observed with $n = 11$ to 13 water molecules ~7.62–7.85 Å (Figure S6, Supporting Information). As observed in the case of 10 water clusters, the separation of

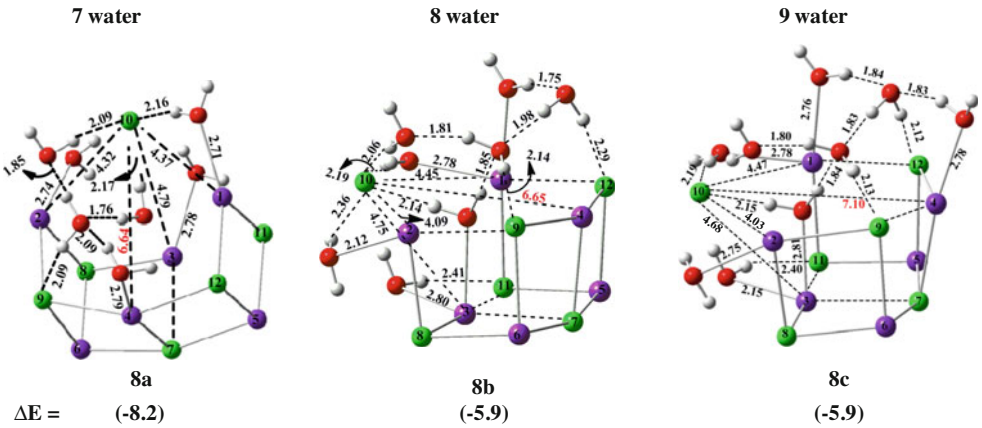


**Fig. 8** B3LYP/6-311 + G(2d,p)//GGA/PW91/DND calculated geometries and binding energies (ΔE) of $(KCl)_6(H_2O)_7$, $(KCl)_6(H_2O)_8$, $(KCl)_6(H_2O)_9$ are given in kcal. Binding energies are calculated with Eq. 1. All distances are given in Å (potassium—*purple*; chlorine—*green*; oxygen—*red*; hydrogen—*white*)

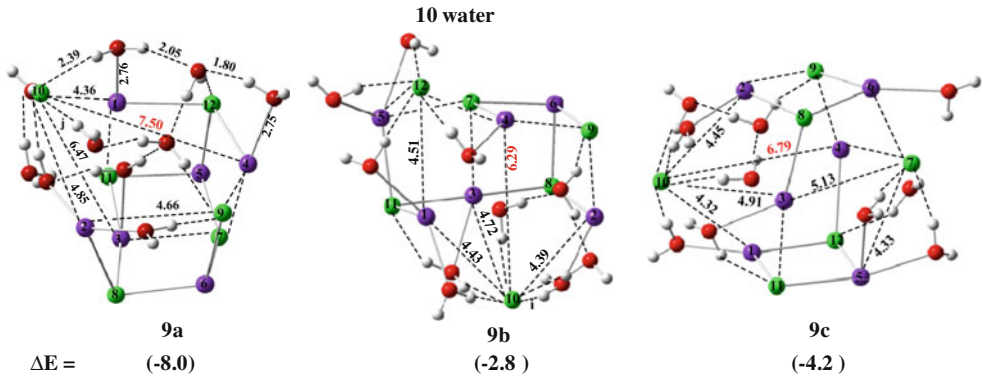


**Fig. 9** B3LYP/6-311 + G(2d,p)//GGA/PW91/DND calculated geometries and binding energies (ΔE) of $(KCl)_6(H_2O)_{10}$ are given in kcal/mol. Binding energies are calculated with Eq. 1. All distances are given in Å (potassium—*purple*; chlorine—*green*; oxygen—*red*; hydrogen—*white*)

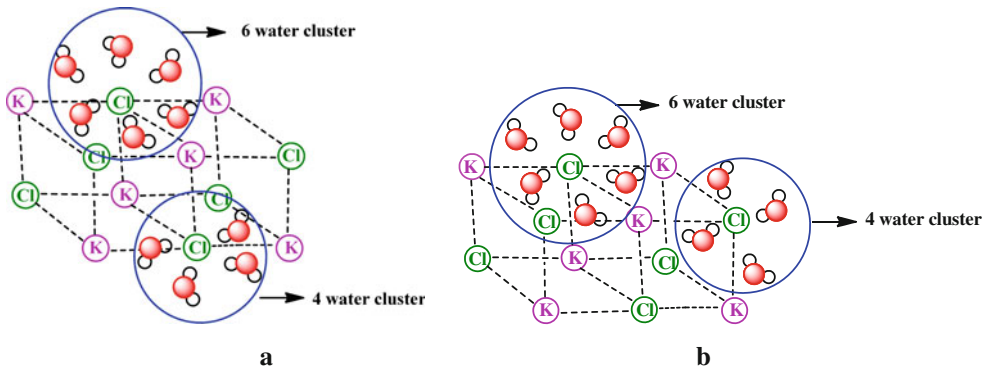


**Scheme 3** The two possible approach of 4 and 6 water clusters toward the KCl microcrystal **a** on two diagonal edge chloride ions and **b** one edge and another corner chloride ion

ions from the microcrystal seems to be less pronounced with the approach of water molecules from different sites (Scheme 3). The separation of $Cl^-$ ions is found to be largest for 10a (8.08 Å) from the edge position of the microcrystal with 14 water molecules (Fig. 10). The calculated results performed with 15 water molecules showed very similar hydrated structure 10b (Fig. 10). The hydrated forms of these KCl microcrystals showed the separation of more polarizable $Cl^-$ ions from the lattice [79], whereas the $K^+$ ions are less perturbed on the lattice sites.

The separation of $Cl^-$ ion from the crystal lattice was also observed with the dissolution process of NaCl [23]. The metadynamics study of Liu et al. using PBE exchange–correlation functional incorporated in the CP2K/Quickstep package showed that the first step of the dissolution of the NaCl starts with an elongation of the corner

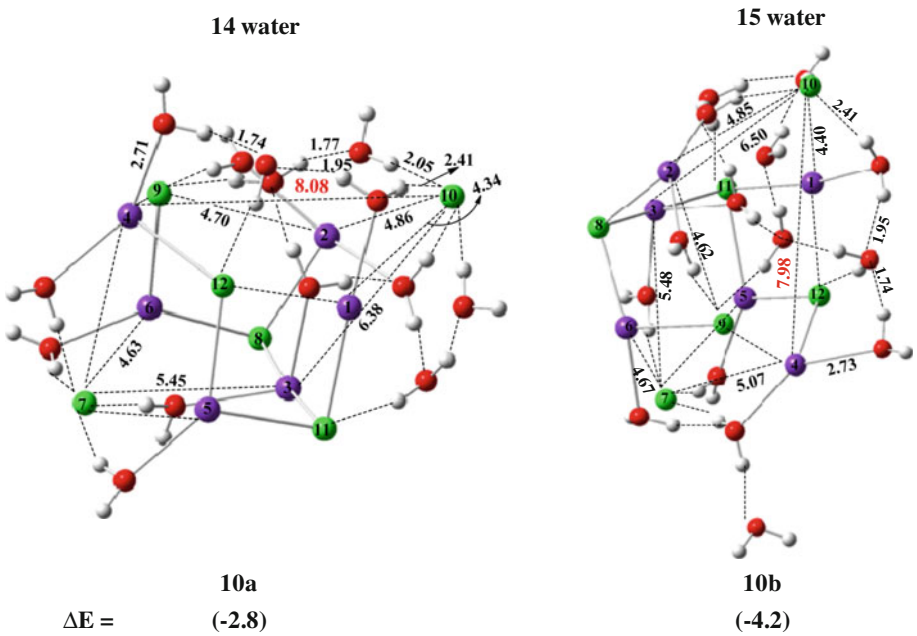


**Fig. 10** B3LYP/6-311 + G(2d,p)//GGA/PW91/DND calculated geometries and binding energies (ΔE) of $(KCl)_6(H_2O)_{14}$ and $(KCl)_6(H_2O)_{15}$ are given in kcal/mol. Binding energies are calculated with Eq. 1. All distances are given in Å (potassium—*purple*; chlorine—*green*; oxygen—*red*; hydrogen—*white*)

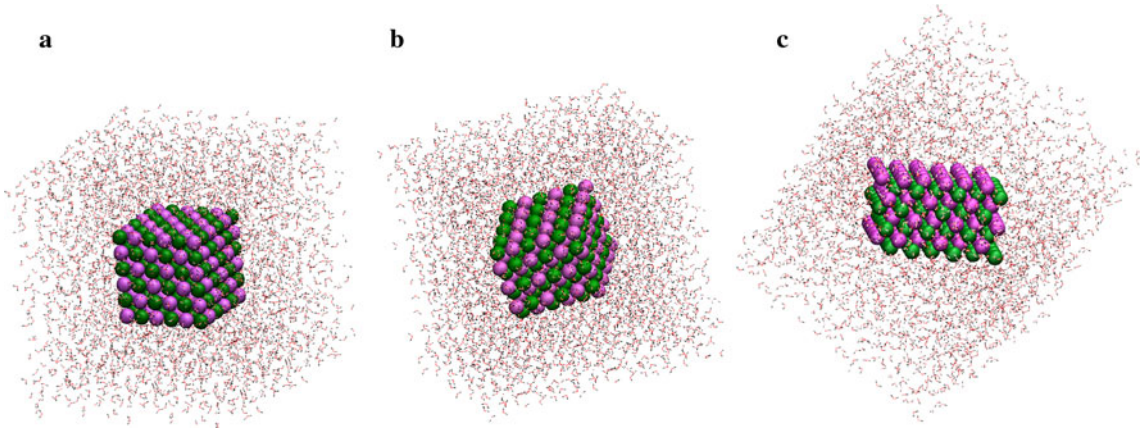


**Fig. 11** The initial structures of the KCl crystals for the MD calculations **a** {100} plane; **b** {110} plane; and **c** {111} plane generated from the crystal structure of KCl. The water molecules are shown surrounding the different planes of the crystals (*green*: chloride; *purple*: potassium; *red*: oxygen and *black*: hydrogen)

$Cl^-$ ion from the lattice, whereas the $Na^+$ ions resides in the crystal lattice. The metadynamics study further showed that $Na^+$ in the form of adatom-like configuration is the second ion to be separated from the NaCl lattice. Thus, this study revealed that the electrical neutrality is conserved in the dissolution of NaCl.

The DFT calculation performed at B3LYP/6-311 + G(2d,p)//GGA/PW91/DND level of theory showed a clear departure of $Cl^-$ ion from the KCl crystal lattice. The DFT calculations are performed with water clusters, and hence in contrast to the metadynamics calculations for NaCl crystals in bulk water [23], the complete dissolution of ions from the KCl lattice was not observed. Interestingly, the use of water clusters shows the initiation of separation of $Cl^-$ ion from the KCl crystal lattice with 4 water molecules, whereas such information is not easy to attain with other approach. The separations of $Cl^-$ ions from the KCl crystal through water clusters are more prominent from the edge of the lattice, which however, was observed from the corner site of NaCl crystal [23]. Furthermore, the elongated $Cl^-$ ion is coordinated with 5 water molecules in most of the cases of $[(KCl)_6(H_2O)_{n=1-15}]$, which was also observed in the NaCl metadynamics study [23].

As stated above, on average, 15 water molecules are necessary to dissociate a single KCl molecule at 273 K at saturation concentration (Supporting Information, Scheme S1), and the DFT calculations also showed a well-separated $K^+$ and $Cl^-$ ions in microcrystal lattice with ~15 water

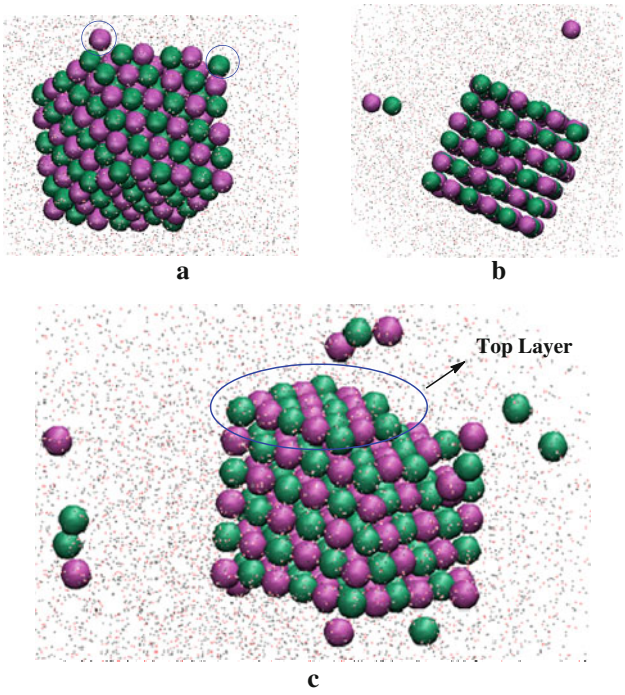


**Fig. 12** Snapshots at **a** 50 ps, **b** 653 ps and **c** 2.5 ns for the molecular dynamics study of {100} plane with $(KCl)_{216}$ and 3248 water molecules are given here. The separating $K^+$ and $Cl^-$ ions at 50 ps are indicated by circles. The water molecules as point structures are shown surrounding the {100} plane of the KCl crystal (*green*: chloride; *purple*: potassium; *red*: oxygen and *black*: hydrogen)

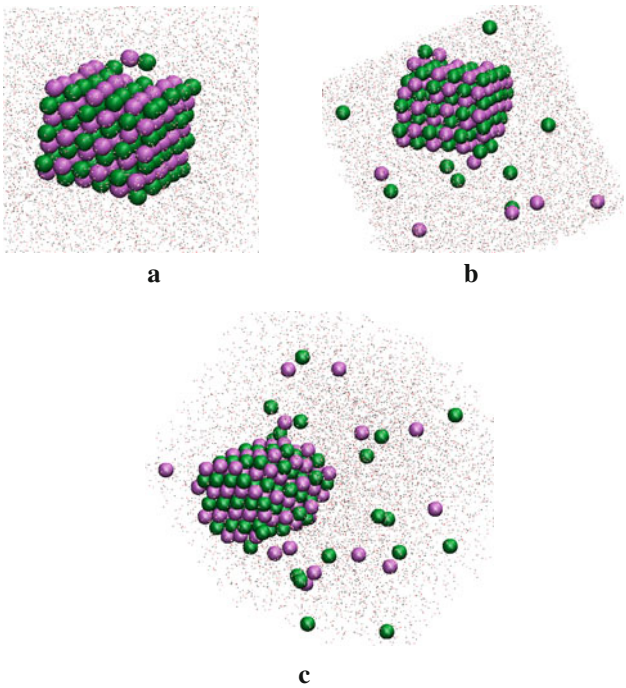


**Fig. 13** Snapshots at **a** 12 ps; **b** 1,000 ps and **c** 2.5 ns for the molecular dynamics study of {110} plane of $(KCl)_{210}$ microcrystal with 3,249 water molecules are given here (*green*: chloride; *purple*: potassium; *red*: oxygen and *black*: hydrogen)

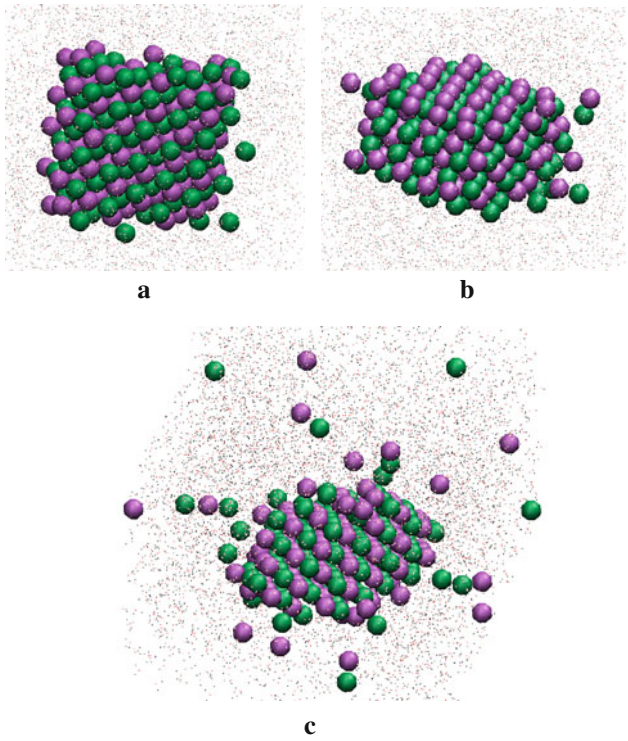


**Fig. 14** Snapshots at **a** 1 ps; **b** 3 ps and **c** 2.5 ns for the molecular dynamics study of {111} plane of $(KCl)_{240}$ microcrystal with 3238 water molecules are given here (*green*: chloride; *purple*: potassium; *red*: oxygen and *black*: hydrogen)

molecules; however, the complete dissolution of such lattice may require more number of water molecules. To examine the dissolution of KCl microcrystal, classical molecular dynamics simulations are performed.

### 3.2 Molecular dynamics study

The DFT calculations predicted the departure of more polarized $Cl^-$ ions from the crystal lattice, with edge sites being more significant than corner sites. However, DFT calculations are static in nature, and thus dynamic study of separation of ions will shed further light on the dissolution of KCl microcrystal. The DFT studies showed the formation of solvent-shared ion pairs (with water clusters containing 3–9 water molecules) and solvent-separated ions (with water clusters of 10–15 water molecules) while interacting with different clusters of water molecules. Nevertheless, the complete dissolution of the ions from the KCl microcrystal lattice in the bulk solution was not achieved. To examine the dynamical profiles of the KCl crystal with larger number of water molecules, we have performed classical NPT MD with GROMOS96 43a1 force field with the GROMACS 3.3.2 program [58, 59]. The molecular dynamics calculations have been performed with a {100} plane of the (KCl) crystal with explicit water

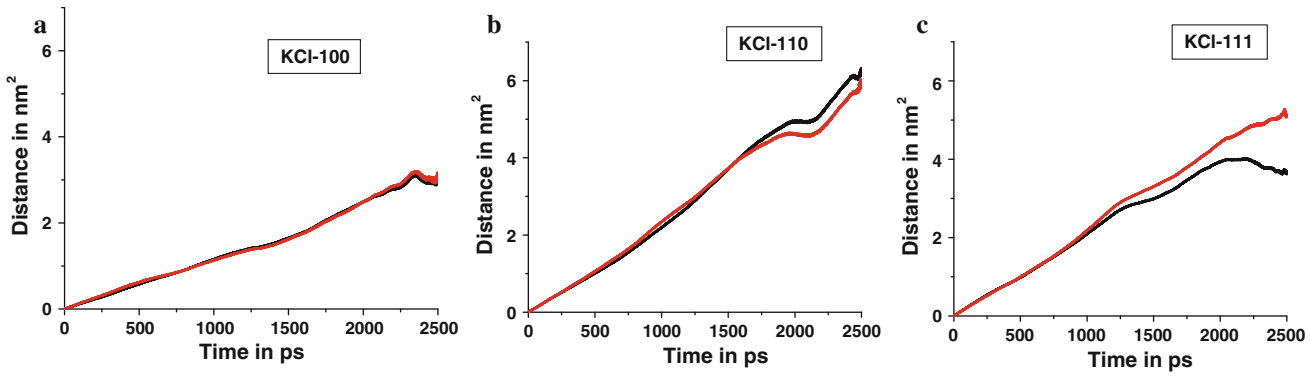


**Fig. 15** Time-dependent mean square displacement of $K^+$ (*black line*) and $Cl^-$ (*red line*) ions in the different planes **a** {100}; **b** {110} and **c** {111}

molecules using TIP4P solvation model. The {100}, {110} and {111} planes of KCl crystal taken for the MD simulation have been given in Fig. 11. The unstable planes {110} and {111} of alkali halides can be grown with the habit modifications of salt crystals [63–65, 80–84].

### 3.2.1 KCl {100} surface

Figure 12 shows the progression of dissolution process of the $(KCl)_{216}$ crystal lattice for the {100} plane at different time steps. The $Cl^-$ and $K^+$ ions seem to separate from the crystal lattice from the different corners of the crystal (a, Fig. 12). We have also noticed that the MM approach does not show a clear preference of $Cl^-$ ion dissolution from the crystal lattice in contrast to the DFT calculations. This difference seems to arise due to the fact that MM force fields do not account for the polarization difference between the ions as observed by Liu et al. [23]. At slightly longer time steps ($\sim$653 ps), the well-separated ion pair and a solvated $K^+$ ion are observed (b, Fig. 12 and Figure S7-S8, Supporting Information). The departures of ions are observed from the different sides of the crystal during the simulations of the {100} plane; however, such ions reabsorb in the lattice at longer time scales. At the completion of the MD run, the dissolved ions separate out only from the top layer of the KCl crystal lattice (c, Fig. 12).

### 3.2.2 KCl {110} surface

Going from KCl {100} plane to the less stable {110} plane, the ion pair initiates to separate from the edge of the lattice (a, Fig. 13). At longer time steps, the ions separate from multiple sites of the {110} plane and the separation of the ions is more pronounced compared to the {100} plane (b and c, Fig. 13). This result suggests that the unstable {110} plane dissolves earlier than the corresponding {100} plane, which supports the surface energy data of alkali halides [37–41]. The dissolution study of NaCl {001} and {011} surfaces performed with classical MD simulations by Shinto et al. [85] suggests that no ion is dissolved from the surfaces within 10 ps. Our study also revealed that within that time scale, the ions are not dissolved from the KCl surfaces {100} and {110}. However, the dissolution of ions starts after 10 ps. Therefore, it appears that the similar dissolution process can also be seen for NaCl surfaces at longer time scales.

### 3.2.3 KCl {111} surface

The KCl {111} plane showed the separation of 3 $Cl^-$ ions from corner and edge of the crystal lattice during initial MD steps (a, Fig. 14). At $\sim$3 ps, potassium ions separate from the crystal lattice (b, Fig. 14). This observation is very similar to the dissolution of {111} plane of NaCl as noticed by Ohtaki et al. [25]. Moreover, the ions separate out in a random fashion from the lattice at longer time steps (c, Fig. 14).

### 3.2.4 MSD analysis

The MSD calculations performed using the GROMACS 3.3.2 software for the {100) and {110} also showed that the displacements of the ions from their initial positions with time are relatively lower for {100} than {110} and {111} planes (Fig. 15). This indicates that the {110} and {111} plane solvate much faster than the {100} plane.

## 4 Conclusion

We have investigated the solubility and dissociation phenomenon of $(KCl)_6$ microcrystal in the presence of 1–15 water molecules computationally using DFT calculations. Molecular dynamics studies with GROMACS force field

have also been carried out to investigate the solvation of all the three planes of the KCl crystal. The DFT calculations predict the separation of the $Cl^-$ ions from the crystal lattice. This observation is similar to the studies performed with NaCl crystals using ab initio MD. The departure of $Cl^-$ has been found to be more significant from the edge of the KCl microcrystal. At least four water molecules are necessary to initiate the separation of the ions from KCl microcrystal [28]. The simultaneous removal of more than one $Cl^-$ ion seems to be less effective in comparison with the removal of a single $Cl^-$ ion from the KCl surface. The DFT calculations reveal that solvent-shared ion pairs are formed with 3 to 9 water clusters, whereas solvent-separated ion pairs are observed with 10-15 water clusters in the hydration process of KCl microcrystal. Classical molecular dynamics calculations performed with the stable {100} surface containing a cluster of 108 $K^+$ and 108 $Cl^-$ ions revealed that both ions seem to separate from corner sites of the crystal lattice in the initial stages of the simulation process, and solvation of ions occurred from a single layer, while other layers remain intact. The polarizability of ions accounts for the preference for the separation of $Cl^-$ ions from the crystal lattice in DFT studies, which is lacking in the MM force field used for classical MD simulations [23]. MD studies are also performed with other unstable planes of the KCl crystal lattice like {110} and {111}. The separation of ion pair from the crystal lattice is observed with {110} plane, whereas $Cl^-$ ions separate out initially for the {111} plane. At longer time scales, solvated ions or ion pairs separate out from different sites within these crystal lattice and solvates much faster than the stable {100} plane, which is also corroborated with MSD analysis. These observations may also be relevant to studies on the reactivity of atmospheric chemistry. Experimental studies may be warranted to test some of the results presented here.

**Acknowledgments** Authors thank DST, New Delhi, India, for financial support of this work. One of the authors AS is thankful to UGC, New Delhi, India, for awarding senior research fellowship. We thank Prof. Jim Thomas (University of Sheffield, UK) for helping in preparing the manuscript. Authors thank the reviewers for their comments and suggestions that have helped to improve the article.

## References

1. Marcus Y (1985) Ion solvation. Wiley-Interscience, New York
2. Kirk KL (1991) Biochemistry of halogens and inorganic halides. Plenum, New York
3. Desvergne J-P (1997) In: Czarnik AW (ed) Chemisensors of ion and molecular recognition. Kluwer, Dordrecht, p 492
4. Arshadi M, Yamdangi R, Kebarle P (1970) J Phys Chem 74:1475–1482
5. Lisy JM (1997) Int Rev Phys Chem 16:267–289
6. Patwari GN, Lisy JM (2003) J Chem Phys 118:8555–8558
7. Hammer NI, Shin J-W, Headrick JM, Diken EG, Roscioli JR, Weddle GH, Johnson MA (2004) Science 306:675–679
8. Katz AK, Gulsker JP, Blebe SA, Bock CW (1996) J Am Chem Soc 118:5752–5763
9. Glendening ED, Feller D (1995) J Phys Chem 99:3060–3067
10. Feller D, Glendening ED, Woon DE, Feyereisen MW (1995) J Chem Phys 103:3526–3542
11. Lee J, Cho SJ, Mhin BJ, Kim KS (1995) J Chem Phys 102:839–851
12. Lee HM, Kim J, Lee S, Mhin BJ, Kim KS (1999) J Chem Phys 111:3995–4004
13. Lee HM, Tarakeshwar P, Park J, Kolaski MR, Yoon YJ, Yi H-B, Kim WY, Kim KS (2004) J Phys Chem A 108:2949–2958
14. Xantheas SS (1995) J Chem Phys 102:4505–4517
15. Ayotte P, Nielsen SB, Weddle GH, Johnson MA, Xantheas SS (1999) J Phys Chem A 103:10665–10669
16. Cabarcos OM, Weinheimer CJ, Lisy JM, Xantheas SS (1999) J Chem Phys 110:5–8
17. Ault BS (1978) J Am Chem Soc 100:2426–2433
18. Singh NM, Yi HB, Min SK, Park M, Kim KS (2006) J Phys Chem B 110:3808–3815
19. Jungwirth P (2000) J Phys Chem A 104:145–148
20. Jungwirth P, Tobias DJ (2002) J Phys Chem B 106:6361–6373
21. Woon DE Jr, Dunning TH (1995) J Am Chem Soc 117:1090–1097
22. Yamabe S, Kouno H, Matsumura KJ (2000) Phys Chem B 104:10242–10252
23. Liu L-M, Laio A, Michaelides A (2011) Phys Chem Chem Phys 13:13162–13166
24. Asada T, Nishimoto K (1995) Chem Phys Lett 232:518–523
25. Ohtaki H, Fukushima N (1989) Pure Appl Chem 61:179–185
26. Yang Y, Meng S, Wang EG (2006) J Phys Condens Matter 18:10165–10177
27. Du H, Miller JD (2007) J Phys Chem C111:10013–10022
28. Sen A, Ganguly B (2010) J Comput Chem 31:2948–2954
29. Peslherbe GH, Ladanyi BM, Hynes JT (2000) J Phys Chem A 104:4533–4548
30. Beichert P, Finlayson-Pitts BJ (1996) J Phys Chem 100: 15218–15228
31. DeHaan DO, Finlayson-Pitts BJ (1997) J Phys Chem A 101:9993–9999
32. Oum KW, Lakin MJ, DeHaan DO, Brauer T, Finlayson-Pitts BJ (1998) Science 279:74–76
33. Schweitzer F, Magi L, Mirabel P, George C (1998) J Phys Chem A 102:593–600
34. Reichardt C, Welton T (1985) Solvation and solvent effects in organic chemistry, 4th edn. Wiley-VCH, Germany
35. Makov G, Nitzan A (1992) J Phys Chem 96:2965–2967
36. Zubov AV, Zubov KV, Zubov VA (2007) Russ J Appl Chem 80:1249–1255
37. Born M, Stern O (1919) Sitzber Preuss Akad Wiss 48:901
38. Westwood ARC, Hitch TT (1963) J Appl Phys 34:3085–3089
39. Gilman JJ (1960) J Appl Phys 31:2208–2218
40. Livey DT, Murray P (1956) J Am Ceram Soc 39:363–372
41. Bruno M, Aquilano D, Pastero L, Prencipe M (2008) Cryst Growth Des 8:2163–2170
42. Perdew JP, Wang Y (1986) Phys Rev B 33:8800–8802
43. Perdew JP, Wang Y (1992) Phys Rev B 45:13244–13249
44. Becke AD (1996) J Chem Phys 104:1040–1047
45. Perdew JP, Burke K, Ernzerhof M (1996) Phys Rev Lett 77:3865–3868
46. Perdew JP, Burke K, Wang Y (1996) Phys Rev B 54:16533–16539
47. Ziesche P, Kurth S, Perdew JP (1998) Comput Mater Sci 11:122–127
48. Kohn W, Becke AD, Parr RG (1996) J Phys Chem 100:12974–12980

49. Wu Z, Cohen RE, Singh DJ (2004) Phys Rev B 70:104112–104118
50. Materials Studio DMOL3 Version 4.1 Accelrys Inc., San Diego
51. Delley B (1990) J Chem Phys 92:508–517
52. Delley B (2000) J Chem Phys 113:7756–7764
53. Delley B (1996) J Phys Chem 100:6107–6110
54. Lee CT, Wang WT, Parr RG (1988) Phys Rev B 37:785–789
55. Becke AD (1993) J Chem Phys 98:5648–5652
56. McLean AD, Chandler GS (1980) J Chem Phys 72:5639–5648
57. Gaussian 09, Revision B.01, Frisch MJ, Trucks GW, Schlegel HB, Scuseria GE, Robb MA, Cheeseman JR, Scalmani G, Barone V, Mennucci B, Petersson GA, Nakatsuji H, Caricato M, Li X, Hratchian HP, Izmaylov AF, Bloino J, Zheng G, Sonnenberg JL, Hada M, Ehara M, Toyota K, Fukuda R, Hasegawa J, Ishida M, Nakajima T, Honda Y, Kitao O, Nakai H, Vreven T, Montgomery Jr JA, Peralta JE, Ogliaro F, Bearpark M, Heyd JJ, Brothers E, Kudin KN, Staroverov VN, Keith T, Kobayashi R, Normand J, Raghavachari K, Rendell A, Burant JC, Iyengar SS, Tomasi J, Cossi M, Rega N, Millam JM, Klene M, Knox JE, Cross JB, Bakken V, Adamo C, Jaramillo J, Gomperts R, Stratmann RE, Yazyev O, Austin AJ, Cammi R, Pomelli C, Ochterski JW, Martin RL, Morokuma K, Zakrzewski VG, Voth GA, Salvador P, Dannenberg JJ, Dapprich S, Daniels AD, Foresman JB, Ortiz JV, Cioslowski J, Fox DJ, (2010) Gaussian, Inc., Wallingford
58. Huber KP, Herzberg G (1979) Molecular spectra and molecular structure IV: constants of diatomic molecules. Van Nostrand-Reinhold, New York
59. Lindahl E, Hess B, Van Der Spoel D (2001) GROMACS 3.0: a package for molecular simulation and trajectory analysis. J Mol Model 7:306–317
60. van Gunsteren WF, Billeter S, Eising AA, Hünenberger PH, Krüger P, Mark AE (1996) Biomolecular simulation:the gromos96 manual and user guide Zürich:Vdf Hochschulverlag AG an der ETH Zürich
61. Jorgensen W, Chandrasekhar J, Madura JD, Impey RW, Klein ML (1983) J Chem Phys 79:926–935
62. Abascal JLF, Sanz E, García Fernández R, Vegas C (2005) J Chem Phys 122:234511–234519
63. Abascal JLF, Vega C (2005) J Chem Phys 123:234505–234516
64. Singh A, Chakraborty S, Ganguly B (2007) Langmuir 23:5406–5411
65. Khan MAS, Sen A, Ganguly B (2009) Cryst Eng Comm 11:2660–2667 and references within
66. Singh A, Sen A, Ganguly B (2010) J Mol Graph Model 28:413–419 and references within
67. Berendsen HJC, Postma JPM, van Gunsteren WF, DiNola A, Haak JR (1984) J Chem Phys 81:3684–3690
68. Darden T, York D, Pedersen L (1993) Chem Phys 98:10089–10092
69. Essmann U, Perera L, Berkowitz ML, Darden T, Lee H, Pedersen LG (1995) J Chem Phys 103:8577–8593
70. Straatsma TP, Berendsen HJC (1988) J Chem Phys 89:5876–5888
71. Gurtovenko AA, Vattulainen I (2008) J Phys Chem B 112:1953–1962
72. Dennis CG, Marimuthu K, David RN, Jeremy CS (2010) J Chem Theor Comp 6:1390–1400
73. Dimitrios A, David RC, Alberto S (2009) J Phys Chem 113:19591–19600
74. Servaas M, Titus S van E, Carsten K, Arnout C, Bert L de G (2012) J Phys Chem B. doi:10.1021/jp209964a
75. Lide DR (1998) Handbook of chemistry and physics, section 9, 79th edn. CRC Press, Boca Raton, p 23
76. Džidić I, Kebarle P (1970) J Phys Chem 74:1466–1474
77. Yamabe S, Furumiya Y, Hiraoka K, Morise K (1986) Chem Phys Lett 131:261–266
78. Langer S, Pemberton RS, Finlayson-Pitts BJ (1997) J Phys Chem A 101:1277–1286
79. Cooker H (1976) J Phys Chem 80:2078–2084
80. Mullin JW (1993) Crystallization, 3rd edn. Butterworth, London, p 238
81. Beinfait M, Boistelle R, Kern R (1965) In: Kern R (ed) Adsorbtion er Croissance Cristalline. Centre National de la Recherche Scientifique, Paris, p 152
82. Green M (1971) Surf Sci 26:549–556
83. Klug DL (1993) In: Myerson AS (ed) Handbook of industrial crystallization. Butterworth, Montvale, p 65
84. Boistelle R, Simon B (1974) J Cryst Growth 26:140–146
85. Shinto H, Sakakibara T, Higashitani K (1998) J Phys Chem B 102:1974–1981